Experimental and Computational Study of Pincer Complexes of Ruthenium with Py, CO, and N_2 Ligands

Dmitry G. Gusev* and Alan J. Lough†

Department of Chemistry, Wilfrid Laurier University, Waterloo, Ontario N2L 3V5, Canada

Received July 1, 2002

Addition of pyridine to the *syn* and *anti* isomers of *cis*-RuHCl[^{t}Bu$_2$PCH$_2$CH$_2$((*E*)-CH═CH)CH$_2$PBu$^t_2$] (**1**) afforded a single isomer of *trans*,*cis*,*anti*-RuHCl(Py)[^{t}Bu$_2$PCH$_2$-CH$_2$((*E*)-CH═CH)CH$_2$PBu$^t_2$] (**2**), where the *anti* α-HC-RuH configuration was established by a difference NOE experiment. The carbonyl complex RuCl(CO)[CH(C$_2$H$_4$PBu$^t_2$)$_2$] (**3**) was obtained from **2** under CO, and two hydride complexes, RuH(CO)[CH(C$_2$H$_4$PBu$^t_2$)$_2$] (**4**) and RuH(N$_2$)[CH(C$_2$H$_4$PBu$^t_2$)$_2$] (**5**), were prepared from **3** and **1**, respectively, using Li[HBEt$_3$] as the hydride source. Decarbonylation of isoamyl alcohol with polymeric [RuCl$_2$(COD)]$_n$ in the presence of 1,5-bis(di-*tert*-butylphosphino)pentane (D^{t}BPP) resulted in isolation of the 16-atom-ring binuclear species [RuHCl(CO)(D^{t}BPP)]$_2$ (**6**). New products **3**−**5** were characterized by single-crystal X-ray analysis. In the computational study, we successfully modeled complexes **1**−**4** using the ONIOM methodology. It was established that the bulky PBu$^t_2$ groups are responsible for the electronically unfavorable *cis* arrangement of the CO and Cl ligands in **3**. B3PW91 calculations of the transition state structures for the intramolecular olefin insertion into the Ru−H bond in *anti*-**1**, *trans*,*cis*-**2**, and *cis*,*trans*-**2** gave barrier heights of 28.3, 27.1, and 17.7 kcal/mol, respectively.

Introduction

Complexes of bulky "pincer" ligands have found important applications in synthesis and catalysis.[1] The simplest diphosphine of this type is 1,5-bis(di-*tert*-butylphosphino)pentane (D^{t}BPP). It was first reported in 1977, and most of the transition metal (Rh, Ir, Pd, and Pt) chemistry with D^{t}BPP was done by Shaw and co-workers some twenty years ago.[2,3] We are studying reactions of bulky diphosphine ligands with ruthenium and osmium[4] and have recently observed dehydrogenation of the alkane chain of D^{t}BPP on ruthenium and formation of the olefin complex RuHCl[^{t}Bu$_2$PCH$_2$CH$_2$((*E*)-CH═CH)CH$_2$PBu$^t_2$] (**1**). Complex **1** has been isolated as a 1:1 mixture of *syn*-**1** and *anti*-**1** isomers distinguished by the *syn* and *anti* configurations of the HC$_\alpha$-RuH fragment, respectively, as shown in Chart 1.[4a] In the present paper we report a convenient high-yield preparation for D^{t}BPP and explore the reactivity of **1**. We also report some structural and dynamic properties of the new products probed by computational methods.

Results and Discussion

Synthesis of D^{t}BPP. Unsatisfactory isolated yields (35 to 50%) were obtained for this ligand in the literature.[2c,k] To develop a convenient one-pot preparation, we studied the reaction of 1,5-dichloropentane with ClPBu$^t_2$ and lithium in THF:

$$\mathrm{Cl(CH_2)_5Cl} + 2\ \mathrm{ClPBu^t_2} + 4\ \mathrm{Li} \rightarrow \mathrm{Bu^t_2P(CH_2)_5PBu^t_2} + 4\ \mathrm{LiCl}$$

With dichloropentane to ClPBu$^t_2$ ratios less than 3:2, formation of D^{t}BPP was observed along with the known diphosphine Bu$^t_2$P-PBu$^t_2$,[5] and the amount of the latter significantly increased as the ratio decreased to the stoicheometric 1:2. With a 3-fold excess of dichloropen-

* Corresponding author. E-mail: dgoussev@wlu.ca.
† Address: X-Ray Laboratory, Department of Chemistry, University of Toronto, Toronto, Ontario, M5S 3H6 Canada.

(1) Recent reviews: (a) Albrecht, M.; van Koten, G. *Angew. Chem., Int. Ed.* **2001**, *40*, 3750. (b) Vigalok, A.; Milstein, D. *Acc. Chem. Res.* **2001**, *34*, 798. (c) Jensen, C. M. *Chem. Commun.* **1999**, 2443. (d) Rybtchinski, B.; Milstein, D. *Angew. Chem., Int. Ed.* **1999**, *38*, 870.

(2) (a) Empsall, H. D.; Hyde, E. M.; Markham, R.; McDonald, W. S.; Norton, M. C.; Shaw, B. L.; Weeks, B. *Chem. Commun.* **1977**, 589. (b) Al-Salem, N. A.; Crocker, C.; Errington, R. J.; McDonald, W. S.; Odell, K. J.; Shaw, B. L. *Chem. Commun.* **1979**, 498. (c) Empsall, H. D.; Markham, R.; Shaw, B. L.; Weeks, B. *J. Chem. Soc., Dalton Trans.* **1979**, 1972. (d) Crocker, C.; Errington, R. J.; Markham, R.; Moulton, C. J.; Odell, K. J.; Shaw, B. L. *J. Am. Chem. Soc.* **1980**, *102*, 4373. (e) Al-Salem, N. A.; McDonald, W. S.; Markham, R.; Norton, M. C.; Shaw, B. L. *J. Chem. Soc., Dalton Trans.* **1980**, 59. (f) Crocker, C.; Empsall, H. D.; Errington, R. J.; Hyde, E. M.; McDonald, W. S.; Markham, R.; Norton, M. C.; Shaw, B. L.; Weeks, B. *J. Chem. Soc., Dalton Trans.* **1982**, 1217. (g) Briggs, J. R.; Constable, A. G.; McDonald, W. S.; Shaw, B. L. *J. Chem. Soc., Dalton Trans.* **1982**, 1225. (h) Crocker, C.; Errington, R. J.; Markham, R.; Moulton, C. J.; Shaw, B. L. *J. Chem. Soc., Dalton Trans.* **1982**, 387. (i) Errington, R. J.; McDonald, W. S.; Shaw, B. L. *J. Chem. Soc., Dalton Trans.* **1982**, 1829. (j) Errington, R. J.; Shaw, B. L. *J. Organomet. Chem.* **1982**, *238*, 319. (k) Timmer, K.; Thewissen, D. H. M. W.; Marsman, J. W. *Rec. Trav. Chim. Pays-Bas* **1988**, *107*, 248.

(3) (a) Seligson, A. L.; Trogler, W. C. *Organometallics* **1993**, *12*, 738. (b) McLoughlin, M. A.; Flesher, R. J.; Kaska, W. C. *Organometallics* **1994**, *13*, 3816. (c) Vigalok, A.; Ben-David, Y.; Milstein, D. *Organometallics* **1996**, *15*, 1839. (d) Vigalok, A.; Milstein, D. *Organometallics* **2000**, *19*, 2061.

(4) (a) Gusev, D. G.; Lough, A. J. *Organometallics* **2002**, *21*, 2601. (b) Gusev, D. G.; Maxwell, T.; Dolgushin, F. M.; Lyssenko, M.; Lough, A. J. *Organometallics* **2002**, *21*, 1095. (c) Gusev, D. G.; Dolgushin, F. M.; Antipin M. Yu. *Organometallics* **2001**, *20*, 1001. (d) Gusev, D. G.; Dolgushin, F. M.; Antipin, M. Yu. *Organometallics* **2000**, *19*, 3429. (e) Gusev, D. G.; Madott, M.; Dolgushin, F. M.; Lyssenko, K. A.; Antipin, M. Yu. *Organometallics* **2000**, *19*, 1734.

(5) (a) Brunelle, J. A.; Bushweller, C. H.; English, A. D. *J. Chem. Phys.* **1976**, *80*, 2598. (b) Aime, S.; Harris, R. K.; McVicker, E. M.; Fild, M. *J. Chem. Soc., Dalton Trans.* **1976**, 2144.

10.1021/om0205142 CCC: $22.00
Publication on Web 10/11/2002

Chart 1

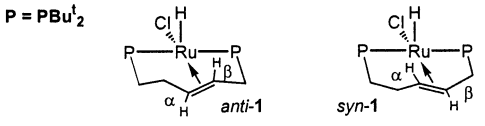

Scheme 1[a]

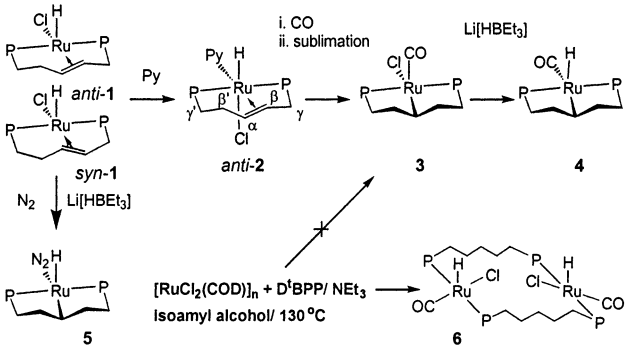

[a] P = PBu$^t_2$.

tane, the ^{31}P NMR spectrum of the reaction solution showed almost quantitative formation of D^{t}BPP, which could be isolated by distillation in 83% yield.

The mechanism of D^{t}BPP formation in this system is unclear, although the intermediacy of radicals can be suspected. Without dichloropentane, the reaction of ClPBu$^t_2$ with lithium in THF proceeded with a great evolution of heat and afforded a single product, the dimer Bu$^t_2$P-PBu$^t_2$. It appears that in the mixture of all three reactants, formation of D^{t}BPP competes with that of Bu$^t_2$P-PBu$^t_2$, and an excess of dichloropentane is needed to produce more D^{t}BPP. The inexplicable property of this system, however, is that despite the presence of a significant excess of the dichloride, only a trace amount of the monosubstituted product, Bu$^t_2$P-(C_5H_{11}), is produced.

Reactions of *syn*- and *anti*-1. Experimental findings of this work are summarized in Scheme 1.

When the mixture of the *syn* and *anti* isomers of RuHCl[^{t}Bu$_2$PCH$_2$CH$_2$((*E*)-CH=CH)CH$_2$PBu$^t_2$] was dissolved in pyridine-d_5 at room temperature, the NMR spectra showed formation of a single isomer of RuHCl(Py)[^{t}Bu$_2$PCH$_2$CH$_2$((*E*)-CH=CH)CH$_2$PBu$^t_2$] (**2**). Yellow, air-stable needlelike crystals of complex **2** were grown from a pyridine−hexane solvent mixture; unfortunately they proved unsuitable for X-ray analysis.

The structure of **2** was elucidated by spectroscopic means. The ^{31}P{^{1}H} NMR spectrum of **2** is similar to that of **1** and exhibits doublets at δ 81.5 and −4.1 ($^2J_{PP}$ = 300.7 Hz) due to the phosphorus atoms in the 5- and 4-atom rings, respectively. ^{1}H, ^{13}C, and {H, C}HETCOR NMR experiments demonstrated the presence of the hydride (δ −9.92, dd, $^2J_{HP}$ = 15.6, 22.8 Hz) and two olefinic CH groups in **2** resonating at δ ^{1}H 4.74, ^{13}C 67.8 (α-CH) and δ ^{1}H 2.57, ^{13}C 38.8 (*β*-CH). The relative HC$_\alpha$-RuH configuration in **2** was found to be *anti* by difference NOE experiments in pyridine-d_5, which showed no NOE between α-CH and the hydride, and a substantial NOE between RuH and *β*-CH. Using a CD_2Cl_2 solution of **2**, we observed a strong NOE between the hydride and *ortho*-CH of coordinated pyridine, whereas there was no NOE between protons of the D^{t}BPP backbone and the Py ligand (Figure 1). The structure

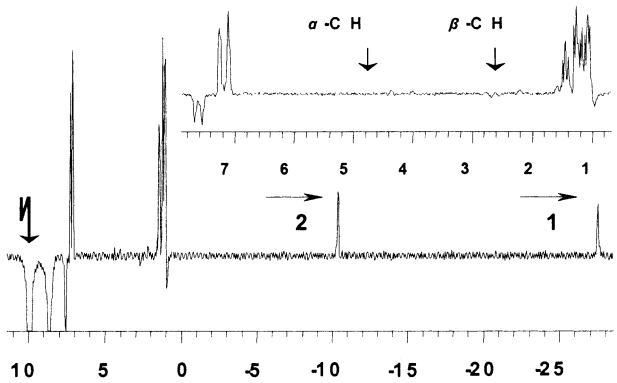

Figure 1. Difference ^{1}H NOE spectrum of **2** in CD_2Cl_2. An arrow at δ 10 indicates the irradiated *o*-CH resonance of coordinated pyridine. In this sample, fast reversible dissociation of pyridine from **2** resulted in formation of *anti*-**1**, as discussed in the text. This figure shows the enhancements of the hydride resonances of **1** and **2** and the absence of NOE between the irradiated *o*-CH resonance and protons of the D^{t}BPP backbone. Resonances between δ 7 and 10 are due to coordinated and free C_5H_5N, and those at δ 1−1.5 belong to the CH_3 groups.

of **2** was thus established as *trans,cis,anti*-RuHCl(Py)-[^{t}Bu$_2$PCH$_2$CH$_2$((*E*)-CH=CH)CH$_2$PBu$^t_2$] (Scheme 1).

Formation of *trans,cis*-**2** and not the *cis,trans* isomer of **2** can be rationalized on the basis of the *trans* effects known to increase in the order Py < Cl$^-$ ≪ H$^-$ < H$_2$C=CH$_2$.[6] It appears that binding of the olefinic fragment *trans* to pyridine and not *trans* to chloride (which possesses a stronger *trans* effect) makes a more favorable arrangement. Another significant factor is that the sites above and below the PC$_\alpha$P plane are constrained by the sterically demanding Bu^t groups and are unfavorable for bulky ligands, i.e., would more likely be occupied by a chloride rather than a pyridine ligand. As to the mechanism of formation of *trans,cis*-**2**, it could result from addition of pyridine to a minor isomer of *anti*-**1** in solution, possessing Cl *trans* to hydride.

To address the facile formation of the *anti* isomer of **2** from *syn*-**1**, we prepared a solution of **1** in pyridine-d_5, at −40 °C. The ^{1}H and ^{31}P NMR spectra of this sample, recorded at −40 °C immediately after preparation, showed two AM patterns. One could be easily assigned to the final product *anti*-**2**, and the other might be due to *syn*-**2** (^{1}H δ −15.92, t, $^2J_{HP}$ = 21 Hz; ^{31}P δ 69.7, −22.3, d, $^2J_{PP}$ = 257 Hz). The latter AM pattern decreased in intensity and disappeared on warming to 20 °C. There was also a third species (**2′**) in the sample that constituted 10−5% of the mixture in the temperature range −40 to 20 °C and disappeared in 20 min after warming to 20 °C. The NMR spectra of **2′** were distinguished by the presence of a doublet hydride resonance at δ −11.67 ($^2J_{HP}$ = 21.6 Hz) and two equally intense ^{31}P singlets at δ 93.7 and 33.5. It was further established from the hydride coupled ^{31}P spectrum and by selective ^{31}P decoupling that the hydride at δ −11.67 was coupled to the phosphorus at δ 93.7. The chemical shift of the other phosphorus at δ 33.5 is similar to that of free D^{t}BPP, δ 26.8 ($CDCl_3$).[2k] These observations suggest that coordination of pyridine to *syn*-**1** results in formation of *syn*-**2** followed by intramolecular dis-

(6) Miessler, G. L.; Tarr, D. A. *Inorganic Chemistry*, 2nd ed.; Prentice Hall: New York, 1999.

Scheme 2[a]

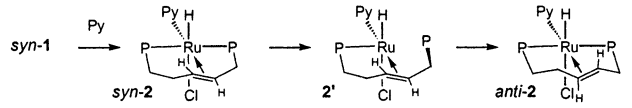

[a] P = PBu^t_2.

Scheme 3[a]

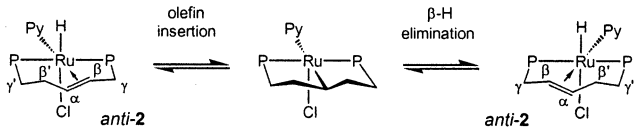

[a] P = PBu^t_2.

sociation of one PBu^t_2 group to give the intermediate **2′** (Scheme 2). It is reasonable to postulate that this complex can be a five-coordinate 16-electron species, as the uncoordinated bulky PBu^t_2 group can protect the vacant site from addition of a second pyridine ligand. We believe that **2′** is fluxional and undergoes a rearrangement to give *anti*-**2**.

Complex **2** is unstable toward pyridine loss, and we studied the reversible dissociation of the ligand in CD_2Cl_2. Formation of an approximately equimolar mixture of **2** and *anti*-**1** was observed at room temperature upon dissolution of **2**. The difference NOE spectrum of the mixture is shown in Figure 1. It exhibits saturation transfer between coordinated and free pyridine and a transfer NOE between the *o*-CH of coordinated pyridine and the hydride of **1**. These features make it evident that the reversible dissociation of the pyridine ligand is fast on the relaxation time scale. In this solution, we also observed a slow isomerization of *anti*-**1** into *syn*-**1**; however it took 2 days before the equilibrium between the two isomers of **1** was established.

Five equilibrium constants for the formation of **2**, $K = [\mathbf{2}][anti\text{-}\mathbf{1}]^{-1}[Py]^{-1}$, were obtained from the ^1H NMR spectra in the temperature range −44 to 39 °C: $\ln(K)/T^{-1} \times 10^3$ = 2.52/3.21, 3.60/3.39, 5.19/3.67, 7.00/3.99, 9.16/4.36. These points show a linear dependence of $\ln(K)$ vs $1/T$, giving the thermodynamic parameters for pyridine addition to *anti*-**1**: $\Delta S = -32$ eu and $\Delta H = -11.4$ kcal/mol.

Performing the NOE experiments in pyridine-d_5, we became aware of the presence of intramolecular pairwise spectroscopic exchange processes in **2** observed as saturation-transfer signals (i.e., in phase with the irradiated partner resonances). Exchange was seen in three H/H pairs: 2.87 (γ-CH)/1.32 (γ′-CH), 2.73 (γ-CH)/0.45 (γ′-CH), and −9.95 (RuH)/2.24 (β′-CH). We could not verify whether there was exchange in the pair 2.57 (β-CH)/2.50 (β′-CH) because of the overlap of the two signals.

Detected saturation was weak at room temperature, at 5−6% of the integral intensity, but increased to 30−40% at 40 °C. For a degenerate exchange process operating on the T_1 relaxation time scale, the rate constant can be evaluated as $k = (1/I - 1)/T_1$, where I is the relative intensity (fraction of the unperturbed intensity) of the resonance affected by saturation transfer and T_1 is its spin−lattice relaxation time.[7] The use of this simplified formula assumes similar T_1 times and negligible mutual dipolar interaction for the exchanging spins, which is true for the H/H pairs in **2**. Our measurements gave the T_1 times of 0.48 s at 23 °C and 0.64 s at 40 °C for the hydride and the T_1 values of 0.40−0.50 and 0.44−0.74 s for the CH_2 and CH protons at the respective temperatures. Thus, the rate constants were estimated as 0.1 s^{-1} at 23 °C and 0.8 s^{-1} at 40 °C, giving the barrier for the dynamic process of 18.5 kcal/mol. We suggest that this process involves reversible intramolecular insertion of the olefinic fragment of **2** into the metal−hydride bond followed by β-hydrogen elimination according to Scheme 3. This mechanism was also invoked to explain exchange between a hydride and olefinic hydrogens in the osmium complex $[OsH_2(H_2C{=}CH_2)(NO)(PPr^i_3)_2]^+$, where a lower barrier of 15 kcal/mol was determined from the NMR spectra at 20 °C.[8]

We attempted trapping with CO the unsaturated intermediates formed when **1** is dissolved in pyridine. However, the ^1H NMR analysis found only a trace amount of pyridine in the solid obtained by evaporation of the pyridine solution of **1** stirred under CO. The ^{31}P NMR spectrum of the product showed three peaks, one of which was subsequently assigned to RuCl(CO)[CH-$(C_2H_4PBu^t_2)_2$] (**3**). The other peaks might be due to dicarbonyl species and were not studied in detail. Sublimation of the product mixture at 210 °C afforded **3** in 86% yield as an air-stable orange solid. The crystal structure of **3** is shown in Figure 2 together with the structures of the carbonyl and dinitrogen complexes, RuH(CO)[CH$(C_2H_4PBu^t_2)_2$] (**4**) and RuH(N_2)[CH$(C_2H_4$-$PBu^t_2)_2$] (**5**), obtained by reacting **3** and **1**, respectively, with Li[$HBEt_3$], according to Scheme 1. Selected bond lengths and angles in **3**−**5** are listed in Table 1, and a summary of the crystallographic data is given in Table 2. Complexes **3**−**5** are isostructural with the related molecules RuCl(CO)[2,6-$(CH_2PBu^t_2)_2C_6H_3$], RuH(CO)[2,6-$(CH_2PBu^t_2)_2C_6H_3$], and RuH(N_2)[2,6-$(CH_2PBu^t_2)_2C_6H_3$].[4d,e]

NMR and IR spectroscopic properties of **3**−**5** are consistent with the crystal structures and are fully reported in the Experimental Section. Two observations deserve comments. One concerns the involvement of the CH groups of **3**−**5** into α-agostic interaction with ruthenium. The one-bond C−H coupling constants $^1J_{CH}$ are 120, 108, and 109 Hz in **3**, **4**, and **5**, respectively, and probably suggest weak α-agostic (η^2-CH)Ru bonding in the two hydride complexes. A medium-intensity band was observed at 2699 cm^{-1} in the IR spectra of **5** in Nujol and KBr that can be assigned to the stretching vibration of an agostic C−H bond. Unfortunately, we failed to detect any agostic C−H vibration in the IR spectra of **4**. The NMR spectra of **3**, **4**, and **5** exhibit CH resonances at δ 1.55, 0.74, 0.97 (^1H) and 59.7, 73.5, 62.8 (^{13}C), respectively. The relatively high-field ^1H shifts and the low-field ^{13}C shifts of **4** and **5** can be due to weak agostic bonding.

Another interesting spectroscopic observation concerns the CO stretching frequencies: 1887 cm^{-1} in the chloride **3** and 1888 cm^{-1} in the hydride **4**. Higher frequency CO stretching vibrations were observed in the isostructural pincer complexes RuCl(CO)[2,6-$(CH_2PBu^t_2)_2C_6H_3$] (1908 cm^{-1}) and RuH(CO)[2,6-

(7) Campbell, I. D.; Dobson, C. M.; Ratcliffe, R. G.; Williams, R. J. P. *J. Magn. Reson.* **1978**, *29*, 397.

(8) Yandulov, D. V.; Bollinger, J. C.; Streib, W. E.; Caulton, K. G. *Organometallics* **2001**, *20*, 2040.

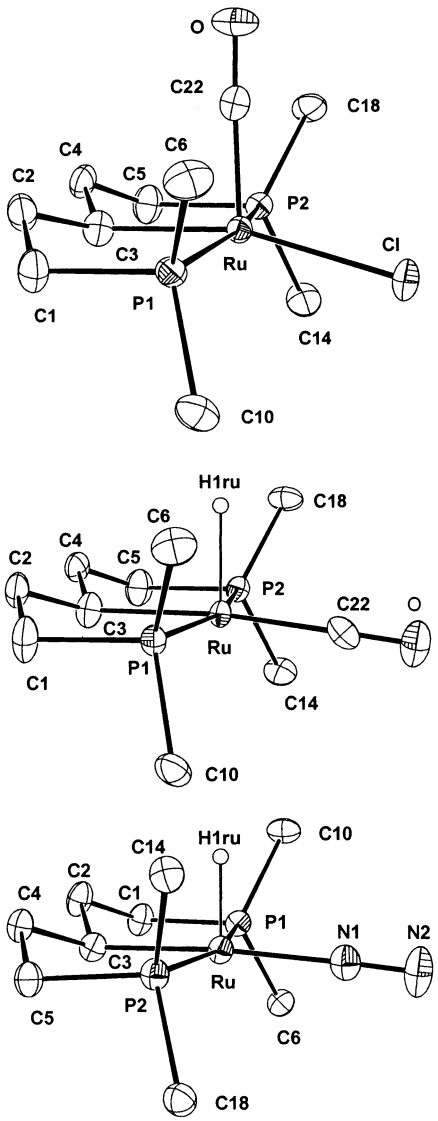

Figure 2. Partial structures of **3**, **4**, and **5** with the ellipsoids set at the 30% probability level.

$(CH_2PBu^t_2)_2C_6H_3]$ (1906 cm^{-1}).[4d,e] The conventional interpretation of these data implies that cyclometalated D^{t}BPP is a better donor than the related pincer ligand, $[2,6\text{-}(CH_2PBu^t_2)_2C_6H_3]^-$. This difference may explain the observation that $RuH_2Cl[CH(C_2H_4PBu^t_2)_2]$ is a Ru(IV) dihydride,[4a] whereas the analogous RuHCl-$[1,3\text{-}(CH_2PBu^t_2)_2C_6H_4]$ is an agostic complex of Ru(II).[4e]

We also attempted preparation of **3** following our earlier method for the carbonyl complex RuCl(CO)$[2,6\text{-}(CH_2PBu^t_2)_2C_6H_3]$, by decarbonylation of isoamyl alcohol with polymeric $[RuCl_2(COD)]_n$ in the presence of the diphosphine ligand.[4e] When this reaction was carried out with D^{t}BPP in isoamyl alcohol, it resulted in a good yield isolation of a yellow, air-sensitive solid of complex **6**. The product was sparingly soluble in dichloromethane (ca. 1 mg/mL) and was insoluble in other common solvents, which made impossible acquisition of a ^{13}C NMR spectrum. We could not crystallize **6** for an X-ray diffraction analysis. An IR spectrum of the isolated solid showed a hydride stretch at 2110 cm^{-1} and two carbonyl peaks at 1910 and 1900 cm^{-1}.

We suggest that **6** might be a diruthenium species with bridging D^{t}BPP ligands, $[RuHCl(CO)(D^tBPP)]_2$. The composition of **6** was confirmed by elemental analysis. Our structural interpretation of **6** in Scheme 4 is based on VT NMR data and is made by analogy with the known 16-atom-ring binuclear species $[RhCl(CO)(D^tBPP)]_2$, which exists in solution as a mixture of rotamers with equivalent and inequivalent phosphorus nuclei.[2b,d]

At room temperature, the ^{31}P NMR spectrum of **6** in CD_2Cl_2 showed two broad lines in a 4:1 ratio at δ 55.1 (**6a**, line width = 36 Hz) and 66.4 (**6b**, line width = 87 Hz). The broadness of the NMR spectra could be attributed to a slow exchange between **6a** and **6b**. Indeed, on lowering the temperature, all resonances sharpened and the ^{31}P line at 55.1 decoalesced into two at δ 55.1 and 55.0. At −20 °C, the peaks at δ 66.4, 55.1, and 55.0 were observed in an approximately 1:2:1 intensity ratio. The resonance at δ 55.1 can be attributed to one of the two structural forms **6a** shown in Scheme 4 and possessing equivalent PBu^t_2 groups. The other rotamer in solution may have the structure **6b** in Scheme 4 and has nonequivalent phosphorus nuclei because the two ruthenium fragments are nonequivalent.

The room-temperature hydride resonance of **6a** was observed as a broadened triplet at δ −24.78 (t, $^2J_{HP}$ = 17.6), and that of **6b** was a very broad line centered at δ −25.1. These shifts are similar to the δ −24.4 shift of the hydride in the square-pyramidal complex RuHCl-$(CO)(PPr^i_3)_2$, where the ligand occupies the apical site.[9] Well-resolved nonequivalent hydride ligands of **6b** were observed at −20 °C at δ −25.06 (t, $^2J_{HP}$ = 17.7) and −25.44 (t, $^2J_{HP}$ = 18.0).

Computational Results

In this section, results of calculations for complexes **3** and **4** are presented first, followed by a computational study of the pyridine complex **2**.

Complex 3. A question that usually arises in modeling complexes with bulky ligands is whether their size can be reduced to lower the computational costs. As it applies to **3**, the first problem we investigated was whether the complex could be modeled as RuCl(CO)-$[CH(C_2H_4PMe_2)_2]$. A DFT calculation on the simplified model established that this approach was inappropriate.

The calculated structure is shown in Figure 3 (left), and selected geometric parameters are listed in Table 3, line 2. Despite some resemblance between the experimental complex **3** and the model RuCl(CO)[CH-$(C_2H_4PMe_2)_2]$, the two have different arrangements of the chloride and carbonyl ligands: Cl is *cis* to CO in **3** and *trans* to CO in the model compound. Interestingly, the optimized Cl−Ru−CO angle of 168.2° in RuCl(CO)-$[CH(C_2H_4PMe_2)_2]$ is in a good agreement with the experimental angle of 167.1° in the complex with monodentate phosphines, $RuCl(CO)(Ph)(PMeBu^t_2)_2$.[10] However, the related pincer complex RuCl(CO)$[2,6\text{-}(CH_2PBu^t_2)C_6H_3]$ possesses chloride *cis* to CO with a Cl−Ru−CO angle of 95.0°.[4e] Apparently, bulky cyclometalated pincer ligands impose constraints that domi-

(9) Esteruelas, M. A.; Werner, H. *J. Organomet. Chem.* **1986**, *303*, 221.
(10) Huang, D.; Streib, W. E.; Bollinger, J. C.; Caulton, K. G.; Winter, R. F.; Scheiring, T. *J. Am. Chem. Soc.* **1999**, *121*, 8087.

Table 1. Selected Bond Distances (Å) and Bond Angles (deg) for Complexes 3, 4, and 5

complex **3**		complex **4**		complex **5**	
Ru−C3	2.100(5)	Ru1−C3	2.153(5)	Ru1−C3	2.114(4)
Ru−C22	1.818(6)	Ru1−C22	1.922(5)	Ru1−N1	1.965(4)
Ru−Cl	2.450(1)	Ru−H1ru	1.70(4)	Ru−H1ru	1.46(3)
Ru−P1	2.389(1)	Ru−P1	2.331(1)	Ru−P1	2.3314(9)
Ru−P2	2.383(1)	Ru−P2	2.329(1)	Ru−P2	2.3285(9)
C22−O	1.150(8)	C22−O	1.092(6)	N1−N2	1.117(5)
C3−Ru−C22	90.3(2)	C3−Ru−H1ru	90.6(15)	C3−Ru−H1ru	91.7(10)
C3−Ru−Cl	163.39(15)	C3−Ru−C22	173.14(18)	C3−Ru−N1	175.46(14)
C3−Ru−P1	82.58(16)	C3−Ru−P1	82.07(13)	C3−Ru−P2	82.30(10)
C3−Ru−P2	82.93(15)	C3−Ru−P2	81.67(13)	C3−Ru−P1	81.87(10)
C22−Ru−Cl	106.26(18)	H1ru−Ru−C22	96.2(15)	H1ru−Ru−N1	92.9(10)
P1−Ru−P2	164.77(5)	P1−Ru−P2	163.71(4)	P1−Ru−P2	163.99(3)

Table 2. Crystallographic Data for Complexes 3, 4, and 5

	3	**4**	**5**
formula	$C_{22}H_{45}ClOP_2Ru$	$C_{22}H_{46}OP_2Ru$	$C_{21}H_{46}N_2P_2Ru$
fw	524.06	489.63	489.63
cryst syst	orthorhombic	orthorhombic	triclinic
space group	*Pbca*	*Pbca*	$P\bar{1}$
a, Å	12.2168(3)	12.0910(1)	8.5134(4)
b, Å	15.5523(3)	15.5600(2)	12.3929(5)
c, Å	26.4565(7)	26.8230(4)	12.8897(7)
α, deg	90	90	101.519(2)
β, deg	90	90	96.208(2)
γ, deg	90	90	105.948(4)
V, Å^3	5026.7(2)	5046.37(11)	1261.93(10)
Z	8	8	2
temp, K	150	150	150
θ min., max., deg	2.62, 25.00	2.73, 27.47	2.68, 27.58
absorp coeff, mm^{-1}	0.868	0.757	0.756
no. of total reflns	37925	39433	13786
no. of unique reflns	4434	5764	5720
R,[a] %	4.71	4.70	4.43
R_w,[a] %	12.41	13.84	10.13

[a] All data collected with Mo Kα radiation ($\lambda = 0.71073$ Å), $R = \sum||F_o| - |F_c||/\sum|F_o|$, $R_w = [\sum(w(F_o^2 - F_c^2)^2)/\sum(w(F_o^2)^2)]^{1/2}$.

Scheme 4[a]

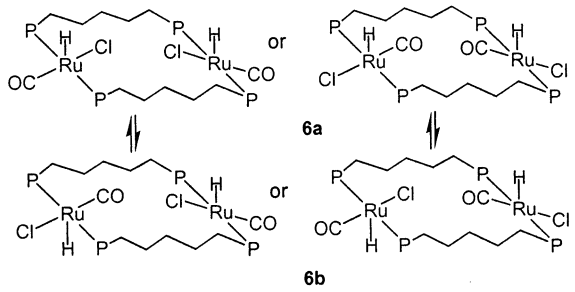

[a] P = PBu^t_2.

nate over the intrinsic electronic preferences of the metal centers.

The structure of **3** was successfully reproduced by ONIOM calculations[11b,c] on the real system RuCl(CO)-$[CH(C_2H_4PBu^t_2)_2]$. The optimized structure of **3**, shown in Figure 3, adopts a slightly distorted square-pyramidal geometry, in which the chloride is displaced from the position *trans* to CO due to repulsion with two *tert*-butyl groups. Rotation of the PBu^t_2 groups is restricted in pincer ligands, making the sites above and below the PCP plane sterically unfavorable for bonding of other ligands.

We carried out several calculations for **3** using combinations of common theoretical methods in the

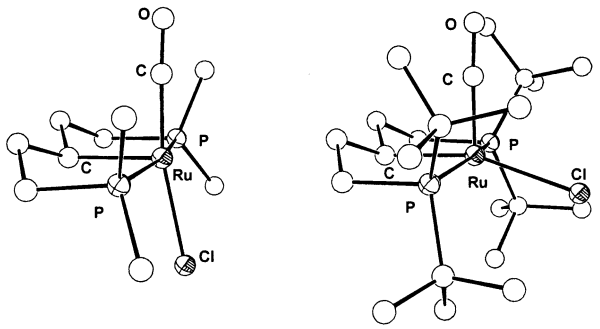

Figure 3. Calculated structures of RuCl(CO)$[CH(C_2H_4PMe_2)_2]$ and RuCl(CO)$[CH(C_2H_4PBu^t_2)_2]$. Their selected bond distances and angles are listed in Table 3, lines 2 and 4, respectively.

ONIOM scheme and summarized the results in Table 3 (lines 3−8). All calculations correctly reproduced the *cis* arrangement of the Cl and CO ligands. Some differences, however, were seen in the quality of the optimized distances and angles compared to the crystallographic data. We note that (i) bond distances calculated with the B3PW91 method were more accurate than those from the B3LYP calculation (cf. lines 3 and 4), (ii) bonds and angles in the "high" level were more accurate when the "low" level (including *tert*-butyl groups) was modeled with the HF rather than with the UFF method, and (iii) the quality of the calculated structure was better when the "high" level included all carbons directly bonded to phosphorus. Therefore, for all subsequent work, the most expedient approach, ONIOM(B3PW91/bs3: UFF) (M1 in Table 3), was employed for preliminary geometry optimizations and was followed by final optimizations at the ONIOM-(B3PW91/bs1: HF/lanl2mb) level (M2 in Table 3) using force constants from the M1 frequency calculations. Only method M1 could be used for modeling the transition structures of this work, because their optimization

(11) (a) Frisch, M. J.; Trucks, G. W.; Schlegel, H. B.; Scuseria, G. E.; Robb, M. A.; Cheeseman, J. R.; Zakrzewski, V. G.; Montgomery, J. A., Jr.; Stratmann, R. E.; Burant, J. C.; Dapprich, S.; Millam, J. M.; Daniels, A. D.; Kudin, K. N.; Strain, M. C.; Farkas, O.; Tomasi, J.; Barone, V.; Cossi, M.; Cammi, R.; Mennucci, B.; Pomelli, C.; Adamo, C.; Clifford, S.; Ochterski, J.; Petersson, G. A.; Ayala, P. Y.; Cui, Q.; Morokuma, K.; Salvador, P.; Dannenberg, J. J.; Malick, D. K.; Rabuck, A. D.; Raghavachari, K.; Foresman, J. B.; Cioslowski, J.; Ortiz, J. V.; Baboul, A. G.; Stefanov, B. B.; Liu, G.; Liashenko, A.; Piskorz, P.; Komaromi, I.; Gomperts, R.; Martin, R. L.; Fox, D. J.; Keith, T.; Al-Laham, M. A.; Peng, C. Y.; Nanayakkara, A.; Challacombe, M.; Gill, P. M. W.; Johnson, B.; Chen, W.; Wong, M. W.; Andres, J. L.; Gonzalez, C.; Head-Gordon, M. E.; Replogle, S.; Pople, J. A. *Gaussian 98W* (Revision A.11) and *GaussViewW*; Gaussian, Inc.: Pittsburgh, PA, 2001. (b) Svensson, M.; Humbel, S.; Froese, R. D. J.; Matsubara, T.; Sieber, S.; Morokuma, K. *J. Phys. Chem.* **1996**, *100*, 19357. (c) Maseras, F. *Chem. Commun.* **2000**, 1821.

Table 3. Experimental and Calculated Bond Distances (Å) and Angles (deg) for Complex 3 (entries in bold are within 0.02 Å or 2° of the experimental distances and angles)

method	Ru−P[a]	Ru−Cl	Ru−C	C−Ru−Cl	C−Ru−C	P−Ru−P	P−Ru−Cl[a]
(1) X-ray	2.386	2.450	1.818; 2.100	106.3; 163.4	90.4	164.8	96.3
(2) B3PW91/bs1[b,c]	2.349	2.416	**1.820**; **2.095**	168.2; 99.4	**92.4**	167.3	90.2
(3) B3LYP/bs1: HF/lanl2mb[c,d]	2.430	2.480	1.776; 2.132	110.0; 158.4	**91.5**	**163.5**	**95.5**
(4) B3PW91/bs1: HF/lanl2mb[c,d] (M2)	**2.405**	**2.454**	1.764; 2.**114**	**108.3**; 160.0	**91.7**	**163.9**	**95.6**
(5) B3PW91/bs2: HF/lanl2mb[e,f]	**2.393**	**2.447**	1.763; **2.120**	112.4; 157.2	**90.4**	**163.4**	**95.6**
(6) B3PW91/bs3: HF/lanl2mb[e,g]	**2.402**	2.473	1.778; 2.129	110.0; 159.4	**90.6**	**163.7**	**95.7**
(7) B3PW91/bs2: UFF[e,f]	2.455	2.423	1.773; **2.118**	100.2; **163.6**	96.2	162.3	**96.7**
(8) B3PW91/bs3: UFF[e,g] (M1)	2.469	**2.446**	1.787; 2.126	96.2; **165.0**	96.2	162.6	**96.8**

[a] Averaged values. [b] Model: RuCl(CO)[CH($C_2H_4PMe_2$)$_2$]. [c] Basis set bs1: SDD + ECP (Ru), 6-31G(d) (CO, C, P, and Cl atoms bonded to Ru), 6.31G (all other C and H atoms). [d] RuCl(CO)[CH($C_2H_4PMe_2$)$_2$] in the high level. [e] RuCl(CO)[CH($C_2H_4PH_2$)$_2$] in the high level. [f] Basis set bs2: polarized (5d) SDD + ECP (Ru, P), 6-31G(d) (CO, C, and Cl atoms bonded to Ru), 6.31G (all other C and H atoms). [g] Basis set bs3: polarized (5d) lanl2dz + ECP (Ru, P, Cl), 6-31G(d) (CO and C atom bonded to Ru), 6.31G (all other C and H atoms).

Table 4. Experimental and Calculated Bond Distances (Å) and Angles (deg) for Complex 4 (entries in bold are within 0.02 Å or 2° of the experimental distances and angles)

method	Ru−P[a]	Ru−H	Ru−C	C−Ru−H	C−Ru−C	P−Ru−P
(1) X-ray	2.330	1.70	1.922; 2.153	96.2; 90.6	173.1	163.7
(2) B3PW91/bs1[b,c]	**2.310**	1.549	1.885; **2.160**	87.2; 99.8	**173.0**	159.6
(3) B3PW91/bs2: UFF[d,e] (M1)	2.368	1.543	**1.913**; **2.163**	87.5; 94.4	178.1	**163.5**
(4) B3PW91/bs3: HF/lanl2mb[f,g] (M2)	**2.348**	1.538	1.876; **2.171**	87.8; 93.0	179.2	**163.7**

[a] Averaged values. [b] Model: RuH(CO)[CH($C_2H_4PMe_2$)$_2$]. [c] Basis set bs1: SDD + ECP (Ru), 6-31G(d, p) (CO and CH groups, P and H atoms bonded to Ru), 6.31G (all other atoms). [d] RuH(CO)[CH($C_2H_4PH_2$)$_2$] in the high level. [e] Basis set bs2: polarized (5d) lanl2dz + ECP (Ru, P), 6-31G(d, p) (hydride, CO and CH groups bonded to Ru), 6.31G (all other C and H atoms). [f] RuCl(CO)[CH($C_2H_4PMe_2$)$_2$] in the high level. [g] Basis set bs3: SDD + ECP (Ru), 6-31G(d, p) (CO and CH groups, P and H atoms bonded to Ru), 6.31G (all other atoms).

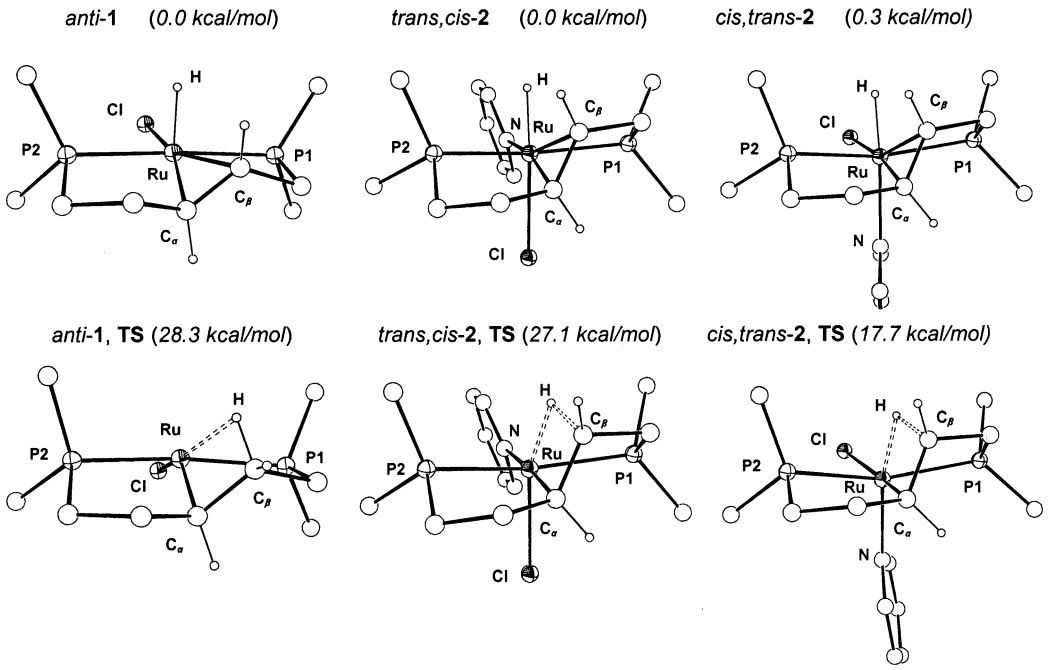

Figure 4. Optimized geometries of the ground and transition structures of complexes *anti*-**1**, *trans*,*cis*-**2**, and *cis*,*trans*-**2**. Most of the hydrogen atoms and all methyl groups are not shown for clarity. The energies are from single-point B3PW91 calculations, and all values for **2** are relative to that for *trans*,*cis*-**2** (see Experimental Section for details).

required time-consuming calculations of force constants in every step (keyword opt=calcall in Gaussian).

Complex 4. The monohydride **4** was optimized at the M1 and M2 levels. Selected bond distances and angles for **4** are listed in Table 4, where theoretical data for the small model RuH(CO)[CH($C_2H_4PMe_2$)$_2$] are also included for comparison. All calculations correctly reproduced the experimental geometry, particularly the *cis* arrangement of the hydride and carbonyl ligands. The reason the size of the phosphine is relatively unimportant for **4** is because the coordination geometry is dominated by the strong *trans* influence of the hydride that takes up the apical position and forces other metal-bonded atoms to adopt a distorted planar arrangement (C−Ru−C = 173.1°, P−Ru−P = 163.7°). The resulting square-pyramidal geometry allows the bulky *tert*-butyl groups to be favorably accommodated above and below the PCP plane, as seen in Figure 2.

Complexes 1 and 2. Figure 4 shows the structures of *anti*-**1**, *trans*,*cis*-**2**, and *cis*,*trans*-**2** optimized at the M2 level; selected bond distances and angles are listed in Table 5. Major structural features of *anti*-**1** are well reproduced by the calculation. The only significant disagreement is seen in the Ru−C distances, which are longer in the crystal structure. There is also a minor inconsistency in the Ru−P bond lengths, which were

Table 5. Experimental and Calculated Bond Distances (Å) and Angles (deg) for *anti*-1 and Calculated Data for *trans,cis*-2 and *cis,trans*-2

model	Ru−H	Ru−$C_{\alpha,\beta}$	C_α−C_β	Ru−$P_{1,2}$	Ru−Cl	Ru−N	H−Ru−Cl	N−Ru−Cl	P−Ru−P
anti-**1**, X-ray	1.53	2.213; 2.312	1.404	2.346; 2.349	2.403		95.1		171.5
anti-**1**[a]	1.529	2.173; 2.191	1.406	2.375; 2.386	2.409		93.5		175.6
trans,cis-**2**[b]	1.569	2.183; 2.186	1.404	2.442; 2.393	2.594	2.193	172.8	88.2	166.6
cis,trans-**2**[b]	1.547	2.160; 2.148	1.416	2.438; 2.364	2.476	2.373	80.7	87.2	164.4

[a] Computational method: ONIOM(B3PW91: bs1/HF: lanl2mb) with $RuHCl[Me_2PCH_2CH_2((E)\text{-}CH{=}CH)CH_2PMe_2]$ in the high level. Basis set bs1: SDD + ECP (Ru), 6-31G(d, p) (H, P, Cl atoms and CH groups bonded to Ru), 6.31G (all other atoms). [b] Computational method: ONIOM(B3PW91: bs2/HF: lanl2mb) with $RuHCl(NC_5H_5)[Me_2PCH_2CH_2((E)\text{-}CH{=}CH)CH_2PMe_2]$ in the high level. Basis set bs2: SDD + ECP (Ru), 6-31G(d, p) (H, N, P, Cl atoms and CH groups bonded to Ru), 6.31G (all other atoms).

Table 6. Calculated Bond Distances (Å) and Angles (deg) for the Transition Structures *anti*-1 TS, *trans,cis*-2 TS, and *cis,trans*-2 TS

model	Ru−H	C_β−H	Ru−$C_{\alpha,\beta}$	C_α−C_β	Ru−$P_{1,2}$	Ru−Cl	Ru−N	N−Ru−Cl	C_α−Ru−Cl
anti-**1 TS**[a]	2.278	1.127	2.082; 2.537	1.524	2.386; 2.382	2.330			138.8
trans,cis-**2 TS**[b]	1.818	1.286	2.098; 2.282	1.466	2.495; 2.445	2.492	2.300	90.3	84.8
cis,trans-**2 TS**[b]	1.695	1.379	2.125; 2.209	1.462	2.525; 2.404	2.541	2.182	86.6	170.5

[a] Computational method: ONIOM(B3PW91: bs1/UFF) with $RuHCl[H_2PCH_2CH_2((E)\text{-}CH{=}CH)CH_2PH_2]$ in the high level. Basis set bs1: polarized (5d) lanl2dz + ECP (Ru, P, Cl), 6-31G(d, p) (hydride and CH groups bonded to Ru), 6.31G (all other atoms). [b] Computational method: ONIOM(B3PW91: bs2/UFF) with $RuHCl(NC_5H_5)[H_2PCH_2CH_2((E)\text{-}CH{=}CH)CH_2PH_2]$ in the high level. Basis set bs2: polarized (5d) lanl2dz + ECP (Ru, P, Cl), 6-31G(d, p) (H, N, and CH groups bonded to Ru), 6.31G (all other atoms).

systematically overestimated by the calculations on all complexes **1**, **3**, and **4**.

The structures of the two isomers of **2** are similar, and *trans,cis*-**2** is slightly (0.3 kcal/mol at the B3PW91 level and 0.9 kcal/mol at the B3LYP level) more stable than *cis,trans*-**2**, in qualitative agreement with the solution NMR data. An important difference between *anti*-**1** and the isomers of **2** is seen along the P1−Ru−P2 axis. From this point of view, the conformation of the two PBu^t_2 groups in *anti*-**1** can be described as eclipsed, since the C_γ−P1−P2−$C_{\gamma'}$ dihedral angle is only 13°. The empty site of *anti*-**1** is occupied by two bulky *tert*-butyl groups, which is a common feature of the square-pyramidal complexes of this work. The absence of an empty site in the octahedral **2** forces the *tert*-butyl substituents to spread as best as they can "between" the hydride, chloride, and pyridine ligands. Therefore, the PBu^t_2 groups of the octahedral **2** adopt a staggered conformation, with C_γ−P1−P2−$C_{\gamma'}$ dihedral angles of 55° in *trans,cis*-**2** and 48° in *cis,trans*-**2**. The orientation of the *tert*-butyl groups on P2 relative to the ligand framework is similar in *anti*-**1** and **2**; that is, the staggered conformation of **2** is due to clockwise rotation of the P(1)Bu^t_2 group. Consequently, the H−Ru−C_α−C_β dihedral angle is reduced from 55° (*anti*-**1**) to 30° in *trans,cis*-**2** and 31° in *cis,trans*-**2**. The hydride···C_β distance is shortened from 2.45 Å (*anti*-**1**) to 2.33 Å in *trans,cis*-**2** and 2.24 Å in *cis,trans*-**2**. The Ru−C_β bond distances follow the same trend: 2.191 Å (*anti*-**1**) > 2.186 Å (*trans,cis*-**2**) > 2.148 Å (*cis,trans*-**2**).

The proximity of C_β to the Ru−H fragment is a feature that correlates with the ease of H−C_β bond formation. Optimized transition structures for the insertion processes in *anti*-**1** and **2** are shown in Figure 4, and selected bond distances and angles are compiled in Table 6. The structure of *anti*-**1 TS** is 28.3 and 28.7 kcal/mol above the ground state at the B3PW91 and B3LYP levels, respectively, in qualitative agreement with the fact that olefin insertion is slow and could not be detected in solution of **1** by NMR spectroscopy. The relative energy of *trans,cis*-**2 TS** is 27.1 and 29.1 kcal/mol above the ground state at the B3PW91 and B3LYP levels, respectively. The transition structure *cis,trans*-**2 TS** is 17.4 and 20.5 kcal/mol above *trans,cis*-**2** at the B3PW91 and B3LYP levels, respectively; these values are in agreement with the experimental activation energy of 18.5 kcal/mol.

Chart 2

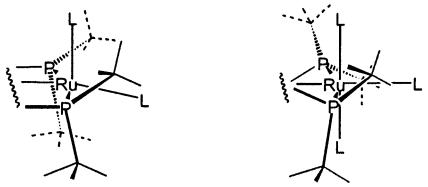

A fast equilibrium between *trans,cis*-**2** and *anti*-**1** and pyridine in a dichloromethane solution was demonstrated by NMR spectroscopy (Figure 1). It seems plausible that there should also be a fast reversible formation of the minor, unobservable isomer *cis,trans*-**2** from *anti*-**1** and pyridine, i.e., effectively, an equilibrium between *trans,cis*-**2** and *cis,trans*-**2**. This solution behavior and the computational results suggest that the reversible olefin insertion observed in *trans,cis*-**2**, may actually be occurring in the minor isomer, *cis,trans*-**2**.

Conclusion

Pincer complexes of ruthenium show preference for five-coordination and square-pyramidal geometry where the PBu^t_2 groups adopt an eclipsed conformation and two *tert*-butyl substituents occupy the empty coordination site, as schematically shown in Chart 2. The bulkiness of the PBu^t_2 groups makes addition of a sixth ligand to the metal center unfavorable. The octahedral complex of this work, $RuHCl(Py)[^tBu_2PCH_2CH_2((E)\text{-}CH{=}CH)CH_2PBu^t_2]$, is unstable in solution and tends to dissociate either the pyridine ligand or one of the phosphorus atoms. As illustrated in Chart 2, the PBu^t_2 groups are staggered in the six-coordinate structure to distribute the *tert*-butyl substituents between the coordinated ligands.

Experimental Section

General Comments. All manipulations were performed under nitrogen using standard Schlenk techniques and a

drybox, where the anhydrous solvents were stored and used. FT IR spectra were recorded on a Perkin-Elmer Spectrum BXII spectrometer. NMR measurements were done on a Varian UNITY Inova 300 spectrometer. Throughout this paper, the NMR data are reported with the apparent coupling of observed virtual triplets (vt) denoted as ^{v}J. All chemicals were obtained from Aldrich. The hydride complex RuHCl[^{t}Bu$_2$PCH$_2$CH$_2$((*E*)-CH=CH)CH$_2$PBu$^{t}_2$] (**1**) was prepared according to a published method.[4a]

Bu$^{t}_2$P(CH$_2$)$_5$PBu$^{t}_2$. Lithium (1.65 g, 0.238 mol, granules, high sodium grade) was added to a solution of ClPBu$^{t}_2$ (10 g, 55.4 mmol) and 1,5-dichloropentane (11.7 g, 83.0 mmol) in THF (50 mL) in a reaction flask equipped with a reflux condenser. Reaction started upon (and required) vigorous stirring and proceeded with moderate warming. Stirring continued for 15 h at room temperature, then under reflux for an additional 3 h. Subsequent treatment could be done in two ways: (a) THF was removed under vacuum, hexane (ca. 20 mL) was added, and the mixture was washed with three portions of water (total 50 mL) to destroy unreacted lithium and remove lithium chloride, or (b) after addition of methanol (2 mL) all volatiles were removed under vacuum, the residue was dispersed in 10 mL of hexane and vacuum-filtered, washing the solids with hexane (filtration can be slow). Both methods were followed by evaporation and drying of the resultant liquid under vacuum for 1 h. The product was isolated by distillation under vacuum of an oil pump, collecting the fraction boiling above 129 °C. Yield: 8.32 g (83%) of a viscous colorless liquid that was at least 98% pure D^{t}BPP.

***trans,cis*-RuHCl(Py)[^{t}Bu$_2$PCH$_2$CH$_2$((*E*)-CH=CH)-CH$_2$PBu$^{t}_2$] (2).** The hydride **1** (0.4 g, 0.81 mmol) was dissolved in 6 mL of pyridine. After addition of 10 mL of hexane and cooling to −16 °C overnight, a light yellow solid crystallized from the solution. The mother liquor was removed with a pipet, and the solid was rinsed with 3 × 1.5 mL of hexane and dried in vacuo for 1 h. Yield: 0.23 g (50%). Anal. Calcd for $C_{26}H_{50}ClNP_2Ru$ (575.17): C, 54.29; H, 8.76; N, 2.44. Found: C, 54.46; H, 8.78; N, 2.48. IR (Nujol): ν(RuH) 2164 cm^{-1}. ^{1}H{^{31}P} NMR (pyridine-d_5): δ −9.95 (s, 1H, Ru*H*), 0.45 (ddd, $^2J_{HH}$ = 14.6, $^3J_{HH}$ = 14.6, 6.8, 1H, γ'-C*H*$_2$), 1.32 (m, 1H, γ'-C*H*$_2$), 1.08, 1.25, 1.28, 1.36 (s, 36H, Bu^{t}), 2.24 (dd, $^2J_{HH}$ = 14.1, $^3J_{HH}$ = 6.7, 1H, β'-C*H*$_2$), 2.50 (m, 1H, β'-C*H*$_2$), 2.57 (m, 1H, β-C*H*), 2.73 (dd, $^2J_{HH}$ = 14.7, $^3J_{HH}$ = 7.0, 1H, γ-C*H*$_2$), 2.87 (dt, $^2J_{HH}$ = 14.7, $^3J_{HH}$ = 2.2, 1H, γ-C*H*$_2$), 4.74 (m, 1H, α-C*H*). ^{1}H{^{31}P} NMR (CD$_2$Cl$_2$): δ 7.12, 7.55, 9.44 (5H, C_5H_5N). ^{13}C{^{1}H} DEPT NMR (pyridine-d_5): δ 17.7 (d, ^1J = 16.4, γ'-*C*H$_2$), 29.1, (d, ^2J = 10.1, β'-*C*H$_2$), 30.6, 30.9, 31.0, 31.1 (d, ^2J = 4.0, *C*H$_3$), 31.6 (d, ^1J = 20.1, γ-*C*H$_2$), 38.8 (d, ^2J = 10.1, β-*C*H), 67.8 (s, α-*C*H). ^{31}P{^{1}H} NMR (pyridine-d_5): δ 81.5, −4.1 (d, $^2J_{PP}$ = 301.7).

RuCl(CO)[CH(C$_2$H$_4$PBu$^{t}_2$)$_2$] (3). A solution of **1** (0.4 g, 0.81 mmol) in 6 mL of pyridine was stirred for 30 min under CO. Then pyridine was removed under vacuum, and the solid residue was dried for 2 h. This afforded 415 mg of a product mixture described in the Results and Discussion section. Further, 362 mg of this solid was sublimed at 210 °C under vacuum of an oil pump to give **3**. Yield: 316 mg (ca. 86%). Sublimed **3** contained ca. 3% of an impurity that showed inequivalent phosphorus resonances at δ 82.2 and 86.6 ($^2J_{PP}$ = 256 Hz) and a characteristic proton resonance at 6.42. These spectroscopic properties are similar to those of Rh(N$_2$)[Bu$^{t}_2$-PCH$_2$(η^1-C=CH)CH$_2$CH$_2$PBu$^{t}_2$],[3d] and the impurity might be the vinyl complex RuCl(CO)[Bu$^{t}_2$PCH$_2$(η^1-C=CH)CH$_2$CH$_2$-PBu$^{t}_2$] produced by dehydrogenation of **3** at 210 °C. In agreement with this assignment, this impurity disappeared from the NMR spectra when the sublimed product was stirred in 2-propanol for 1 min under H$_2$ at 90 °C. Anal. Calcd for $C_{22}H_{45}ClOP_2Ru$ (524.06): C, 50.42; H, 8.65. Found: C, 50.47; H, 8.85. IR (Nujol): ν_{CO} 1887 cm^{-1}. ^{1}H NMR (C$_6$D$_6$): δ 1.18, 1.31 (vt, ^{v}J = 6.6; 36H, C*H*$_3$), 1.31 (m, 2H, γ-C*H*$_2$), 1.55 (m, overlapped, 3H, α-C*H* and β-C*H*$_2$), 1.75 (m, 2H, γ-C*H*$_2$), 2.11 (m, 2H, β-C*H*$_2$). ^{31}P{^{1}H} NMR (C$_6$D$_6$): δ 83.0. ^{13}C{^{1}H} NMR (C$_6$D$_6$): δ 24.2 (vt, ^{v}J = 9.4, γ-*C*H$_2$), 28.7, 29.5 (vt, ^{v}J = 2.3, *C*H$_3$), 35.9, 36.9 (vt, ^{v}J = 7.1, P*C*), 42.0 (vt, ^{v}J = 6.2, β-*C*H$_2$), 59.7 (s, α-*C*H), 211.1 (t, $^2J_{CP}$ = 13.2, *C*O).

RuH(CO)[CH(C$_2$H$_4$PBu$^{t}_2$)$_2$] (4). A 1 M solution of Li[HBEt$_3$] in THF (1.11 g, 1.27 mmol) was mixed with a solution of **3** (335 mg, 0.64 mmol) and NEt$_3$ (130 mg, 1.28 mmol) in THF (3 mL). The reaction mixture was filtered and evaporated. The residue was washed with 5 × 3 mL of methanol and dried under vacuum for 3 h. Yield: 284 mg (91%). Anal. Calcd for $C_{22}H_{46}OP_2Ru$ (489.63): C, 53.97; H, 9.47. Found: C, 53.77; H, 9.27. IR (Nujol): ν_{CO} 1888 cm^{-1}; ν_{Ru-H} 2089 cm^{-1}. ^{1}H NMR (CD$_2$Cl$_2$): δ −28.88 (t, $^2J_{HP}$ = 18.0, 1H, Ru*H*). ^{1}H{^{31}P} NMR (CD$_2$Cl$_2$): δ 0.74 (tt, $^3J_{HH}$ = 12.0, 4.8, 1H, α-C*H*), 1.13, 1.22 (s, 36H, *CH*$_3$), 1.47 (m, 2H, β-C*H*$_2$), 1.74 (ddd, $^2J_{HH}$ = 14.0, $^3J_{HH}$ = 14.0, 6.3, 2H, γ-C*H*$_2$), 2.25 (dd, $^2J_{HH}$ = 14.0, $^3J_{HH}$ = 5.3, 2H, γ-C*H*$_2$), 2.39 (m, 2H, β-C*H*$_2$). ^{31}P{^{1}H} NMR (CD$_2$Cl$_2$): δ 110.2. ^{13}C{^{1}H} NMR (CD$_2$Cl$_2$): δ 27.4 (vt, ^{v}J = 8.8, γ-*C*H$_2$), 29.0, 29.5 (s, *C*H$_3$), 35.1, 36.5 (vt, ^{v}J = 8.3, 6.8, P*C*), 40.5 (vt, ^{v}J = 9.4, β-*C*H$_2$), 73.5 (t, $^2J_{CP}$ = 4.4, α-*C*H), 206.2 (t, $^2J_{CP}$ = 9.1, *C*O).

RuH(N$_2$)[CH(C$_2$H$_4$PBu$^{t}_2$)$_2$] (5). A 1 M solution of Li[HBEt$_3$] in THF (3.77 g, 4.21 mmol) was mixed with a solution of **1** (2 g, 4.03 mmol) in THF (10 mL), under nitrogen. Then, the mixture was stirred for 1 h, filtered, and evaporated. The residue was washed with 4 × 3 mL of ethanol and dried under vacuum for 7 h. Yield: 1.8 g (91%). Anal. Calcd for $C_{21}H_{46}N_2P_2Ru$ (489.63): C, 51.51; H, 9.47; N, 5.72. Found: C, 51.61; H, 9.23; N, 5.50. IR (Nujol): ν 2061, 2075 cm^{-1}. ^{1}H NMR (C$_6$D$_6$): δ −31.56 (t, $^2J_{HP}$ = 18.6, 1H, Ru*H*), 0.97 (m, 1H, α-C*H*), 1.07, 1.23 (vt, ^{v}J = 5.8, 6.2, 36H, *CH*$_3$), 1.50 (m, 4H, β-C*H*$_2$ and γ-C*H*$_2$), 1.99 (m, 2H, γ-C*H*$_2$), 2.42 (m, 2H, β-C*H*$_2$). ^{31}P{^{1}H} NMR (C$_6$D$_6$): δ 100.8. ^{13}C{^{1}H} NMR (C$_6$D$_6$): δ 26.5 (vt, ^{v}J = 8.6, γ-*C*H$_2$), 29.2, 30.0 (vt, ^{v}J = 3.0, 3.5, *C*H$_3$), 35.8, 37.0 (vt, ^{v}J = 7.1, 5.3, P*C*), 41.8 (vt, ^{v}J = 9.5, β-*C*H$_2$), 62.8 (t, $^2J_{CP}$ = 3.6, α-*C*H).

[RuHCl(CO)(Bu$^{t}_2$P(CH$_2$)$_5$PBu$^{t}_2$)]$_2$ (6). A mixture of [RuCl$_2$(COD)]$_n$ (0.37 g, 1.32 mmol), D^{t}BPP (0.5 g, 1.39 mmol), and triethylamine (134 mg, 1.32 mmol) in 10 mL of isoamyl alcohol was stirred for 72 h at 130 °C. This resulted in formation of a yellow solid, which was isolated by filtration, washed with 20 mL of THF and 3 × 3 mL of methanol, and dried in vacuo for 1 h. Yield: 583 mg (84%). Anal. Calcd for (C$_{22}$H$_{47}$OP$_2$Ru)$_2$ (1052.17): C, 50.23; H, 9.00. Found: C, 50.05; H, 8.94. IR (Nujol): ν_{CO} 1900, 1910 cm^{-1}; ν_{Ru-H} 2110 cm^{-1}. ^{1}H NMR (CD$_2$Cl$_2$): δ −24.78 (br t, $^2J_{HP}$ = 17.6, 1H, Ru*H*), 1.35, 1.43 (*CH*$_3$), 1.4−2.0 (featureless m, C*H*$_2$). ^{31}P{^{1}H} NMR (CD$_2$Cl$_2$): δ 55.1 (br s, 77%), 66.4 (br s, 23%).

Computational Details. All calculations were done on a 2.2 GHz Pentium IV PC with Gaussian 98W (Revision A.11) and GaussViewW programs.[11a] All geometries were fully optimized without symmetry or internal coordinate constraints using the ONIOM approach,[11b,c] which included Hartree−Fock and UFF[12] methods in the "low level". In the "high level", B3LYP and B3PW91 methods were used, which are combinations of Becke's three-parameter hybrid functional[13a] with the nonlocal correlation provided by the LYP[13b,c] and by the PW91 expressions.[13d]

The basis sets employed for geometry optimization were 6-31G (augmented by polarization functions on the metal-bonded atoms),[14a,b] LANL2DZ (augmented by 5d polarization functions: α = 0.364 (P), 0.648 (Cl) and associated with the relativistic effective core potentials for Ru, P, and Cl),[14c−e] and SDD from the Stuttgart group (augmented by 5d polarization function on phosphorus (α = 0.397)[14f,g] and associated with the relativistic effective core potentials for Ru and P).[14h] More

(12) Rappé, A. K.; Casewit, C. J.; Colwell, K. S.; Goddard, W. A., III; Skiff, W. M. *J. Am. Chem. Soc.* **1992**, *114*, 10024.
(13) (a) Becke, A. D. *J. Chem. Phys.* **1993**, *98*, 5648. (b) Lee, C.; Yang, W.; Parr, R. G. *Phys. Rev. B* **1988**, *37*, 785. (c) Miehlich, B.; Savin, A.; Stoll, H.; Preuss, H. *Chem. Phys. Lett.* **1989**, *157*, 200. (d) Perdew, J. P.; Burke, K.; Wang, Y. *Phys. Rev. B* **1996**, *54*, 16533.

information on the choice of the basis sets is available from Tables 3−6.

The nature of the stationary points was verified by frequency calculations, which were also used to calculate ZPE without scaling. All transition state structures *anti*-**1 TS**, *trans*,*cis*-**2 TS**, and *cis*,*trans*-**2 TS** were characterized by single imaginary frequencies (NIMAG = 1), while the rest of the optimized structures *anti*-**1**, *trans*,*cis*-**2**, *cis*,*trans*-**2**, **3**, and **4** possessed only real frequencies. For all transition states, motion corresponding to the imaginary frequency was visually checked. All reported energies are ZPE corrected and originate from single-point B3PW91 and B3LYP calculations using the SDD basis set for Ru and the 6-31+G(d, p) basis set for all other atoms.

Acknowledgment. D.G. thanks WLU, NSERC, Ontario Government and Research Corporation, for funding.

Supporting Information Available: Tables of atomic coordinates, bond lengths and angles, and anisotropic thermal parameters for **3**, **4**, and **5**. This material is available free of charge via the Internet at http://pubs.acs.org.

OM0205142

(14) (a) Hariharan, P. C.; Pople, J. A. *Theor. Chim.* Acta **1973**, *28*, 213. (b) Rassolov, V.; Pople, J. A.; Ratner, M.; Windus, T. L. *J. Chem. Phys.* **1998**, *109*, 1233. (c) Hay, P. J.; Wadt, W. R. *J. Chem. Phys.* **1985**, *82*, 299. (d) Wadt, W. R.; Hay, P. J. *J. Chem. Phys.* **1985**, *82*, 284. (e) Check, C. E.; Faust, T. O.; Bailey, J. M.; Wright, B. J.; Gilbert, T. M.; Sunderlin, L. S. *J. Phys. Chem. A* **2001**, *105*, 8111. (f) Dolg, M.; Stoll, H.; Preuss, H.; Pitzer, R. M. *J. Phys. Chem.* **1993**, *97*, 5852. (g) Bergner, A.; Dolg, M.; Küchle, W.; Stoll, H.; Preuss, H. *Mol. Phys.* **1993**, *80*, 1431. (h) Basis sets can be obtained from the Extensible Computational Chemistry Environment Basis Set Database, which is developed and distributed by the Molecular Science Computing Facility, Environmental and Molecular Sciences Laboratory, which is part of the Pacific Northwest Laboratory, P.O. Box 999, Richland, WA 99352.